J. Fluid Mech. (1985), *vol.* 151, *pp.* 337–365
Printed in Great Britain

Modulational development of nonlinear gravity-wave groups

By T. K. CHERESKIN† AND E. MOLLO-CHRISTENSEN‡
Massachusetts Institute of Technology, Department of Meteorology and Physical Oceanography, Cambridge, Massachusetts 02139

(Received 29 April 1983 and in revised form 1 May 1984)

We present observations of the development of nonlinear surface gravity-wave groups. We calculate the amplitude and phase modulations using Hilbert-transform techniques. With increasing propagation distance and wave steepness, the phase modulation develops local phase reversals whose locations correspond to amplitude minima or nodes. The concomitant frequency modulation develops jumps or discontinuities. The observations are compared with recent similar results for wavetrains. The observations are modelled numerically using the cubic nonlinear Schrödinger equation. The motivation is twofold: to examine quantitatively the evolution of phase as well as amplitude modulation and to test the inviscid predictions for the asymptotic behaviour of groups versus long-time observations. Although dissipation rules out recurrence, there is a long-time coherence of the groups. The phase modulation is found to distinguish between dispersive and soliton behaviour.

1. Introduction

This paper examines the long-time evolution of nonlinear surface gravity-wave groups. Observations of the propagation of groups of waves of fixed frequency and amplitude were made in an unusually long wave channel. The purpose of the observations was twofold: to examine quantitatively the evolution of the amplitude and phase modulations and to test the predictions of weakly nonlinear wave theory (cubic Schrödinger equation) for the asymptotic behaviour of wave groups.

The experiments were carried out with the cooperation of Dr M.-Y. Su of NORDA. He has described the qualitative evolution of these wave groups (Su 1982). However, since the early work of Feir (1967) there has not been a study that has calculated the phase and frequency modulations of wave groups, in part owing to lack of a technique with sufficient resolution. We here apply a Hilbert-transform method used successfully by Melville (1983) on wavetrains.

We use the cubic nonlinear Schrödinger (NLS) equation to predict and model the experimental observations. There are two main differences between our use of this model and that of previous work. First, we specify phase as well as amplitude modulation as an initial condition and then compare the subsequent amplitude and phase evolutions with the observations. The initial phase specification does not appear to be crucial for narrow-banded wave-group evolution since the phase is basically uniform. The interesting result is the subsequent evolution; the phase does not remain uniform but exhibits a modulation that provides a clearer indication of the type of

† Present address: College of Oceanography, Oregon State University, Corvallis, Oregon 97331.
‡ Present address: NASA, Goddard Space Flight Center, Greenbelt, Maryland 20771.

nonlinear interaction that occurs than can be seen from amplitude modulation alone. Most previous work examines only the amplitude modulation and ignores the phase.

Secondly, because the observations were made in an unusually long wave channel, they include the cumulative effect of dissipation on the long-time evolution. Previous comparison between the NLS model and observations was not for very long evolution. In a study of wavetrains Lake *et al.* (1977) attempt to achieve a longer effective propagation distance by forcing larger-amplitude initial sidebands. The effect of dissipation on such a wavetrain differs from that on a wavetrain with an initially smaller-amplitude sideband disturbance that has evolved for longer.

The prediction of the inviscid theory for these wave groups indicates the possibility of a bound state of solitons, with recurrent behaviour and long-time coherence for wave groups (Zakharov & Shabat 1972; Satsuma & Yajima 1974). Obviously, exact recurrence cannot occur if dissipation is present. However, if the timescale on which dissipation acts is long enough, then perhaps a quasi-recurrence is possible. Long-time observations are thus needed to observe the timescale on which dissipation acts and to test the predictions of inviscid theory. Dissipation is included in the model in a rather crude form, but one which nevertheless gives good comparison with observation.

2. Experiments

The experiments were very simple in nature: constant-amplitude single-frequency wave groups were generated using a plunger-type wavemaker. The steepness ak varied from weak ($ak = 0.03$) to moderate ($ak = 0.16$) nonlinearity. Three group lengths were used: 10, 15 and 25 waves per group. We use group length to mean group duration or the number of waves at one place; the actual group length is half this number of waves.

The experiments were made in an outdoor wave channel in Bay St Louis, Mississippi. The horizontal dimensions of the channel were 3.66 m × 137.2 m. The sides were constructed of plywood, and the bottom was mown grass. The water depth was 72 cm. The values of kh in these experiments ranged from 2 to 5, which places them marginally at the deep-water limit. The rough bottom acts to increase dissipation above that of a smooth one. However, Su (1982) has repeated the experiments in a deeper (4 ×) indoor channel with a smooth bottom and has found the same qualitative evolution that we see here.

The wavemaker used is of plunger-type with a hyperbolic forward face. The period of the wavemaker is measured at the drive shaft. For these experiments the measurements from 18 wave-height sensors, the wind velocity and the wavemaker period were all recorded on magnetic tape. The experiments were made under still wind conditions. The wave-height sensors were of capacitance type. They were calibrated by raising and lowering them a fixed distance. The sensors were placed along the centreline of the channel, and measurements were made at the following fetches (distance in metres): 6.1, 15.2, 30.5, 45.7, 61.1, 76.2, 91.4, 106.7, 121.9 and 137.2. Most locations had wave-gauge pairs separated by 0.30 m (roughly one quarter-wavelength). The locations of the wave gauge pairs were 6.1, 30.5, 61.1, 91.4, 106.7, 121.9 and 137.2. In addition, a third wave gauge at 121.9 was placed near the sidewall as a check that three-dimensional effects were negligible. The pairs were used to determine the wavenumber.

Experiment	N_w	ak	f_0 (Hz)	k (rad/cm)	f_1 (Hz)	df	$10^5\alpha$ (cm^{-1})
78	10	0.03	0.80	0.025	0.80	0	6
79	15	0.03	0.80	0.025	0.80	0	7
80	25	0.03	0.80	0.025	0.80	0	8
75	10	0.07	0.97	0.036	0.97	0	6
76	15	0.07	0.96	0.036	0.96	0	6
77	25	0.07	0.96	0.036	0.96	0	5
86	10	0.10	0.96	0.037	0.95	0.01	7
87	15	0.10	0.96	0.037	0.95	0.01	7
88	25	0.10	0.96	0.037	0.94	0.02	6
61	10	0.15	1.20	0.060	1.06	0.12	4
62	15	0.15	1.20	0.060	1.04	0.13	4
63	25	0.15	1.21	0.060	1.04	0.14	5
21	10	0.16	1.21	0.050	1.05	0.13	4
22	15	0.16	1.21	0.050	1.02	0.17	6
23	25	0.16	1.21	0.050	1.01	0.16	4

TABLE 1. Experimental parameters

3. Observations

In comparison with continuous wavetrains, the frequency downshifting observed in wavetrains (Lake *et al.* 1977; Melville 1982) and in wind waves (Mollo-Christensen & Ramamonjiarisoa 1982) seems also to occur for isolated groups in the absence of wind. A weakly nonlinear wavetrain is modulationally unstable to sideband perturbations (Benjamin & Feir 1967). The wavetrain is observed to modulate with fetch, then demodulate and reform into a nearly uniform wavetrain, but at slightly lower frequency (Lake *et al.* 1977).

For groups of sufficient steepness ($ak \geqslant 0.10$), wavepackets also exhibit this phenomenon of frequency downshifting. In brief, the downshifting in wave groups seems also to result from a modulational instability. Initially, sidebands to the fundamental are observed to grow. After a time the lower sideband grows at a faster rate than the upper sideband. The modulation is strongest when the lower sideband is still smaller than the fundamental peak. Eventually the lower sideband exceeds the fundamental. At this point, the time development indicates that the modulation has sorted itself into a succession of quasi-permanent solitons with larger-amplitude lower-frequency groups leading. The downshifting process seems irreversible. A distinction to be made between wave groups and wavetrains is that, although the peak downshifts, not all the groups have the downshifted frequency (Su 1982).

The Benjamin–Feir analysis, a linear theory valid for the initial growth, predicts the most unstable sideband frequency f_1 to be linearly related to the wave steepness (d$f = |f_1 - f_0|/f_0 = ak$). The long-term spectral evolution indicates good agreement with the Benjamin–Feir prediction even for moderate nonlinearity and long-term group development. Table 1 summarizes the frequency downshift for various initial wave steepnesses and group lengths. We examine the spectral and the modulational development for an individual experiment in greater detail below.

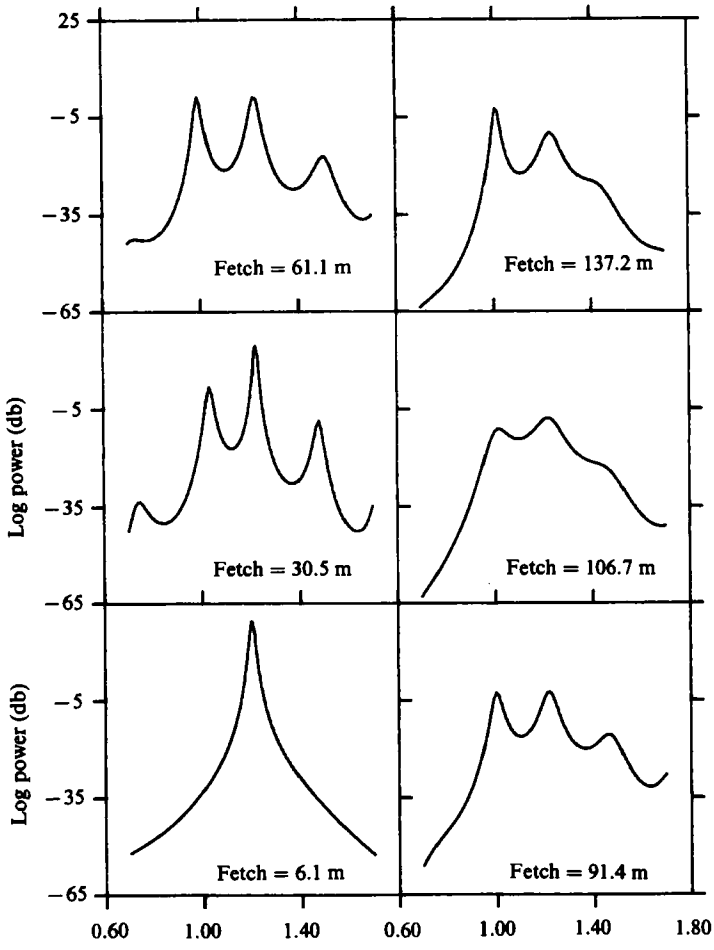

FIGURE 1. Maximum-entropy method (MEM) spectral evolution for a group of 25 waves of initial steepness $ak = 0.16$. Notice the appearance of sidebands at 30.5 m; lower already exceeds upper. At 61.1 m the lower equals the fundamental. At further fetch there is a merging of the lower sideband and fundamental; the new peak frequency is downshifted (16%). There is also a growth of the continuous spectrum.

3.1. *Spectra*

Figure 1 shows the spectral evolution of a group of 25 waves with initial steepness $ak = 0.16$ and carrier frequency $f_0 = 1.2$ Hz. Although this is a rather long group, it is a relatively short time series. Fourier analysis reveals the appearance of new frequencies; however, for short time series (period T) it does not give very good peak resolution ($1/T$).

Here we present maximum-entropy method (MEM) spectral estimates. If auto-regression is a good model for the data, the MEM estimator yields improved peak resolution and spectral fidelity over traditional spectral estimators (Kay & Marple 1981). The data are first bandpassed (in Fourier space) on a 1 Hz frequency interval centred on f_0. The bandpass is used to achieve very good peak resolution close to the carrier. In experiments where downshifting occurred, the width of the interval always included the downshifted frequency. This was checked by comparison with spectra of unfiltered data from the furthest wave observation in the channel.

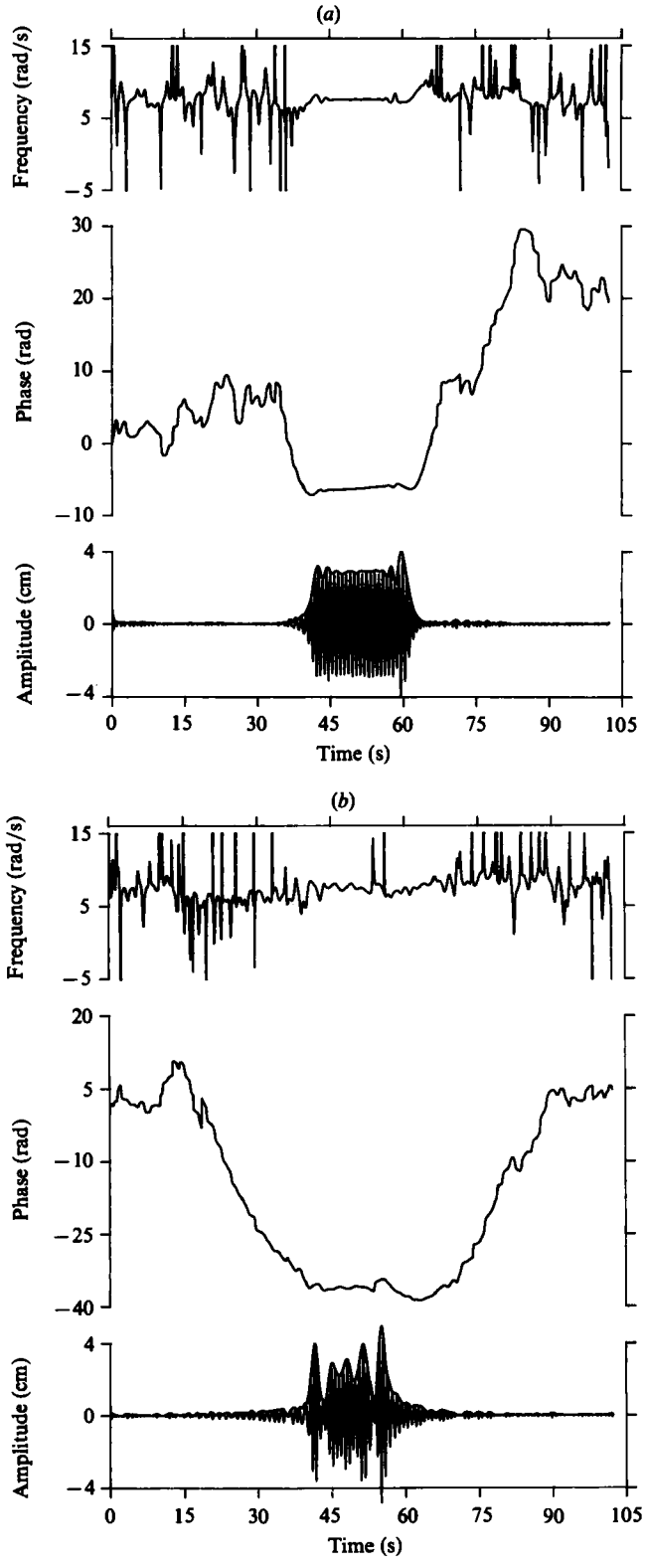

FIGURE 2*a*,*b*. For description see p. 345.

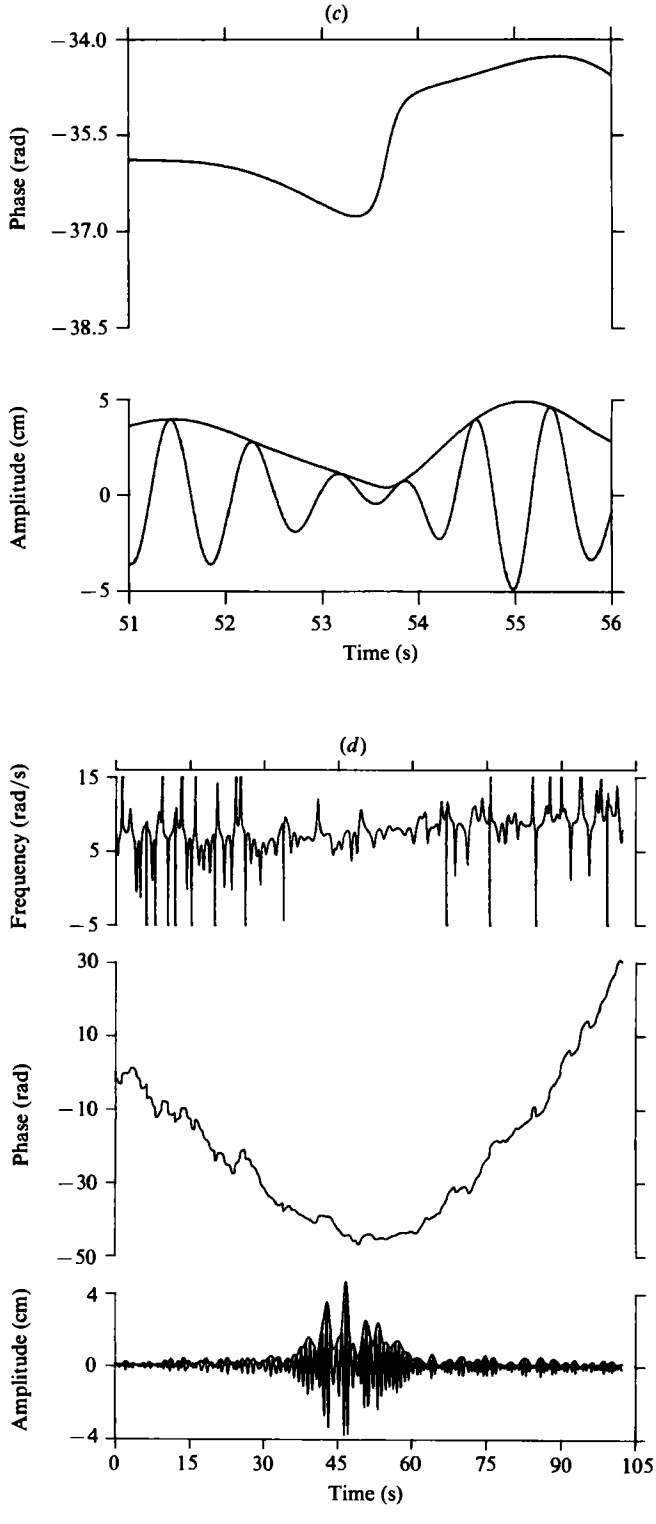

FIGURE 2*c*,*d*. For description see p. 345.

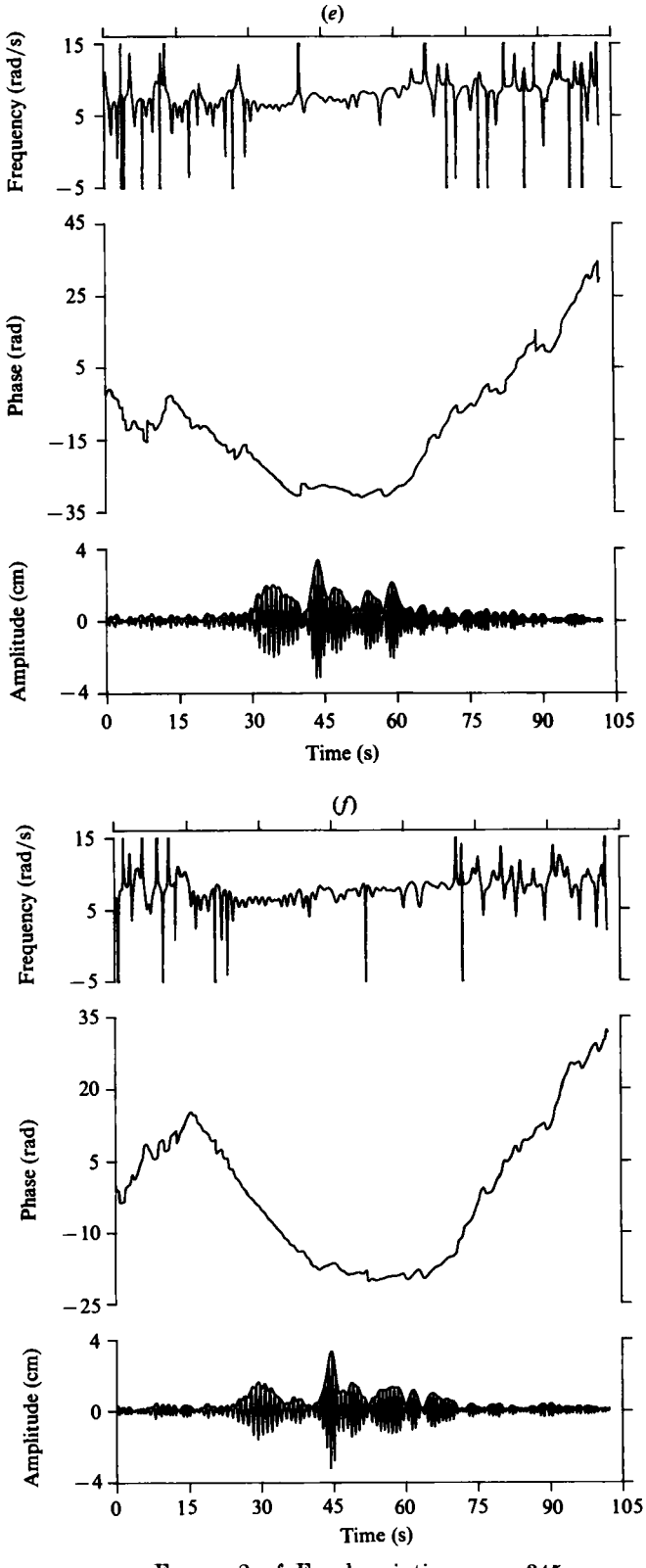

FIGURE 2*e*, *f*. For description see p. 345.

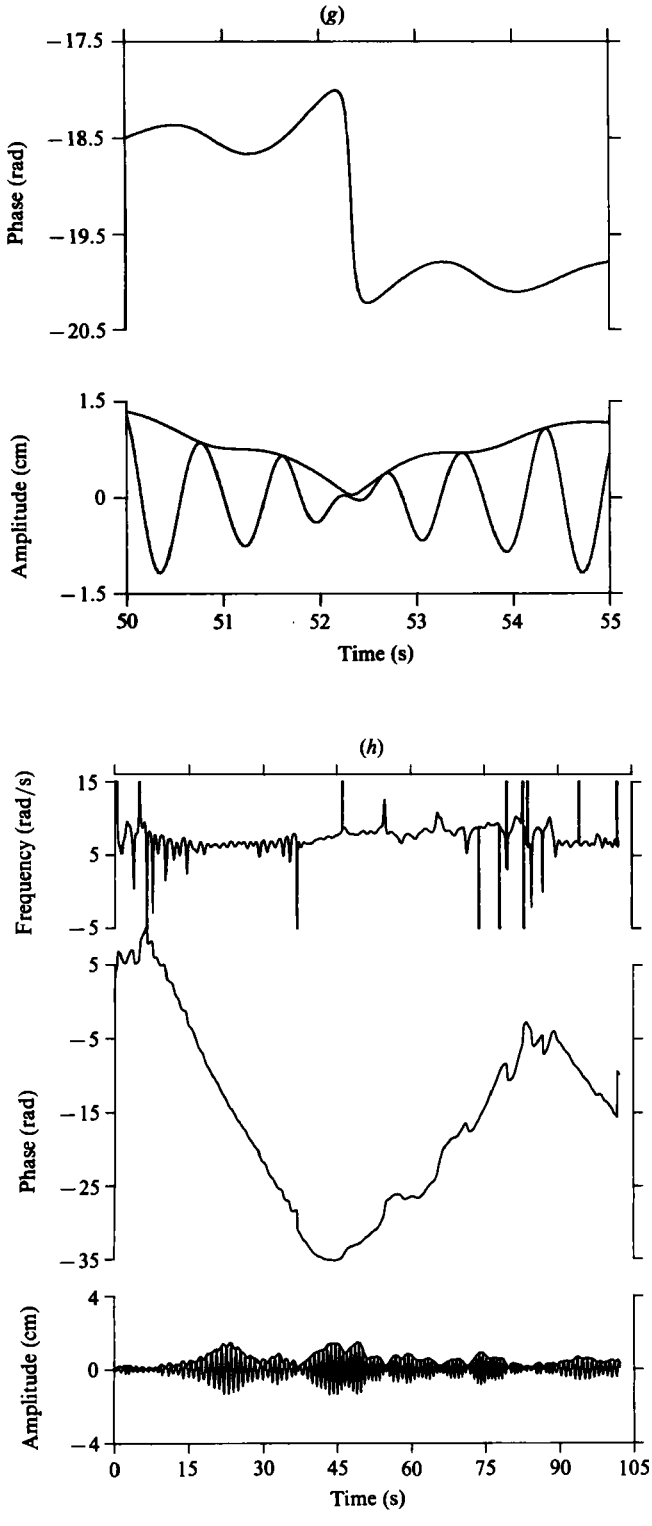

FIGURE 2*g*, *h*. For description see opposite.

The initial peak (at 6.1 m) in figure 1 is quite narrow and is located at 1.2 Hz. Figure 2 shows the time development and the modulation. In figure 2(*a*) we see that the group is slightly modulated at either end. The strongest modulation occurs whilst the sideband perturbations to the carrier are still growing (from 30.5 to 61.1 m). In the time development we see small-amplitude leading low-frequency waves and trailing high-frequency waves disperse away from the central group as it propagates. Once the downshifting occurs (between 106.7 and 137.2 m), the modulation is weaker, and the initial pulse is sorted out into a succession of 4–5 envelope solitons of increasing frequency and decreasing amplitude. The downshifted frequency is 1.01 Hz. The splitting is still incomplete at 137.2 m. Experiments with shorter pulses and smaller steepnesses show that smaller initial disturbances evolve more quickly, in qualitative agreement with theoretical prediction (Zakharov & Shabat 1972).

3.2. *Modulations*

We assume the following model for our wavegauge observations:

$$g(x_i, t) = \mathrm{Re}\{a(x_i, t) \exp[\mathrm{i}(\omega_0 t + \theta(x_i, t))]\}, \tag{3.1}$$

where $g(x_i, t)$ is the measurement of surface displacement at fixed location x_i and ω_0 is the initial (radian) carrier frequency. This models the surface displacement signal as the product of a rapidly varying carrier wave

$$\exp[\mathrm{i}(\omega_0 t)] \tag{3.2}$$

and a slowly varying complex envelope

$$a(x_i, t) \exp[\mathrm{i}\theta(x_i, t)]. \tag{3.3}$$

The amplitude modulation $a(x_i, t)$ and the phase modulation $\theta(x_i, t)$ are obtained using the Hilbert transform of the signal. The frequency modulation is defined as

$$f(x_i, t) = \omega_0 + \frac{\mathrm{d}}{\mathrm{d}t}(\theta(x_i, t)). \tag{3.4}$$

The transform method and its assumptions are documented in Appendix A. The data are bandpassed (the same as for the spectra) on a 1 Hz band centred on the carrier frequency. This is done to achieve a smooth envelope; higher-frequency contributions are not what we consider as part of the slow modulation of the carrier. However, as will be seen below, we note frequencies in the frequency-modulation time series that are outside the passband. These are instantaneous frequencies, i.e. the filtering in Fourier space will not remove any high-frequency fluctuations in the time series that occur over one or two wave periods (typically less).

FIGURE 2. Concomitant amplitude, phase and frequency modulations for a group of 25 waves of initial steepness $ak = 0.16$ at 6 successive fetches. Time origins are arbitrary. (*a*) Modulations at 6.1 m. Amplitude modulation is superimposed over the group. Notice the excellent fit. The phase is unwrapped and is uniform within the group. (*b*) Modulations at 30.5 m. Within the group 2 weak jumps in frequency corresponding to local reversals in phase located at minima in amplitude modulation are shown. (*c*) An expanded view of the first phase reversal (53.7 s) within the group at 30.5 m. The magnitude of the phase change is 2 rad. The amplitude modulation is at a minimum, but is still positive-definite. (*d*)–(*f*) Modulations at 61.1, 91.4, and 106.7 m. Notice frequency modulation jumps and phase reversals where amplitude modulation minima occur. (*g*) Expanded view of phase reversal occurring at 52.4 s in the time series at 106.7 m. The magnitude is approximately 2.3 rad and the amplitude modulation goes to zero. This looks very much like a 'crest-pairing' event in which crests merge and the frequency downshifts. (*h*) Modulations at 137.2 m.

Figure 2 shows the amplitude, phase and frequency modulations at six different wave-gauge locations. The amplitude modulation is superimposed on the filtered wave group. Notice the excellent fit. The phase modulation is defined with the initial carrier trend removed and has been unwrapped. The unwrapping technique looks for and removes discontinuities of 2π. These arise from using the principal value of the arctangent to determine the continuous phase modulation.

There is very little phase variation within the group. Most of the phase variation occurs outside the group where the amplitude is nearly zero. Discontinuities (or jumps) in the frequency modulation occur where there are local reversals in phase. Again, there is little variation within the initial group; a small amount develops with fetch. Most of the jumps in frequency (hence reversals in phase) occur where there are local amplitude minima. Where jumps do occur within the wave group, they tend to occur where there is a minimum in amplitude modulation (figures 2*b–h*).

In the observation time series at 30.5 m (figure 2*b*) we see a reversal in phase and a jump in frequency modulation occurring at 53.7 s. Figure 2(*c*) amplifies this phase reversal. The magnitude of the phase change is approximately 2 rad, and it occurs at a local amplitude minimum. Notice that the modulation envelope is greater than zero.

Figure 2(*f*) is an example of a phase reversal occurring later in the evolution, this time at 106.7 m. In the time series of figure 2(*f*) we see a reversal in phase and a jump in frequency occurring at 52.4 s. Figure 2(*g*) shows the magnitude of the jump to be approximately 2.3 rad. The amplitude modulation goes to zero. This looks very much like a 'crest-pairing' event in which crests merge and the frequency downshifts.

These jumps are an important and consistent feature of the observations. Their frequency of occurrence within wave groups increases with wave steepness and with wave-group evolution. They have also been observed in continuous wavetrains.

3.3. *Discussion*

Melville (1983) has observed these jumps in a study that examined the evolution to breaking of nonlinear surface gravity wavetrains. He computes an instantaneous phase speed, the ratio of measured frequency to wavenumber modulation, and finds small regions of very rapid, large-amplitude variations in phase speed corresponding to the phase reversals. The large gradients or jumps that he observes in the frequency, wavenumber and phase speed always occurred in the neighbourhood of local minima in wave amplitude. Melville suggests that these jumps may be the mechanism of 'crest pairing' (one crest overtakes another and disappears) observed by Ramamonjiarisoa & Mollo-Christensen (1979; and Mollo-Christensen & Ramamonjiarisoa 1982) and the 'loss of crests' observed by Lake & Yuen (1978). Crest pairing may be the visual manifestation of the frequency downshift. These local large phase-speed variations in the vicinity of amplitude minima may act to merge crests or troughs (local instability) and to decrease the frequency.

The spectral evolution gives us information regarding the amplitude but not the phase modulation. Ramamonjiarisoa & Mollo-Christensen (1979) have shown that a phase shift between amplitude and phase modulation results in an asymmetry in the spectrum (as in the asymmetry of the sidebands). Melville (1983) has observed an evolving phase shift between amplitude and frequency modulations in a continuous wavetrain. Initially, he finds no phase lag between amplitude and phase. The shift increases with evolution such that phase leads the amplitude modulation by $\frac{1}{4}\pi$. The modulations evolve from symmetric sinusoidal variations to increasingly asymmetric variations with steep forward faces and more gradually sloping rear faces. When the

amplitude is strongly modulated (extending to nearly zero), large jumps in frequency occur corresponding to small sudden reversals in phase.

An evolving asymmetry of the phase and amplitude modulations implies that the instantaneous nonlinear phase speed also exhibits asymmetry. In addition, if the phase modulation propagates at a different speed than the amplitude modulation (evolving phase shift), then these small regions of anomalously large phase-speed variation are propagating through the group. These narrow regions involving a large jump in phase speed, with larger phase speed overtaking slower, may result in local instability which acts to merge crests (crest pairing) and lower the frequency. Dispersion of the groups with lower frequency may then achieve the observed sorting into a succession of envelope solitons. In continuous wavetrains there would be no sorting but rather a propagating modulation.

4. Model

We model the wave-group observations using the cubic nonlinear Schrödinger (NLS) equation. Zakharov (1968) was the first to derive the two-dimensional cubic NLS equation in the context of deep-water waves. It describes the evolution of the slowly varying complex modulation envelope of gravity waves on deep water. It has been derived and solved by a number of different methods (e.g. Chu & Mei 1970, 1971; Zakharov & Shabat 1972; Yuen & Lake 1975). For a recent review of this equation and its solutions see Peregrine (1983). Our use of this model differs in two respects from that of previous work: we specify the phase as well as the amplitude from observations and compare the subsequent evolution, and we make these comparisons over a long time with both damped and undamped numerical solutions.

We solve the NLS equation using a modified Crank–Nicholson implicit scheme with second-order centred spatial finite-differencing. The scheme and computer code were taken from Yue (1980).

The free-surface deflection η' is represented as the real part of the product of a complex modulation envelope A' and a rapidly varying carrier wave with wavenumber k_0 and frequency ω_0 (primes denote dimensional quantities):

$$\eta'(x',t') = \mathrm{Re}\{A'(x',t')\exp[\mathrm{i}(k_0 x'-\omega_0 t')]\}. \tag{4.1}$$

We non-dimensionalize as follows:

$$X = \epsilon k_0\left(x'-\frac{\omega_0 t'}{2k_0}\right), \quad T = \epsilon^2\omega_0 t', \quad A = \frac{kA'}{\epsilon}, \tag{4.2}$$

where $\epsilon = k|A'|$ is the wave steepness. The equation governing the complex modulation envelope can be shown to be (see e.g. Yuen & Lake 1975)

$$\mathrm{i}A_T - \tfrac{1}{8}A_{XX} - \tfrac{1}{2}|A|^2 A = 0. \tag{4.3}$$

This equation is valid to $O(\epsilon^2)$. The theory assumes weak nonlinearity, narrow-bandedness (slow variations of frequency and wavenumber about their mean values which are small compared with amplitude variation) and inviscidness.

The equation is solved subject to the boundary condition

$$|A| \to 0 \quad \text{as } X \to \infty. \tag{4.5}$$

An infinity of conservation laws exists for the NLS equation. We compute our error at each time step by using the first law

$$C_1 = \int_{-\infty}^{\infty} |A|^2 \,\mathrm{d}X. \tag{4.6}$$

The transformation from a spatial evolution in the wave-channel frame of reference to a temporal evolution in the numerical frame for both the initial condition and further comparison with observations was accomplished using linear group velocity. This transformation has been employed by Benjamin & Feir (1967), Chu & Mei (1970, 1971), and Lake *et al.* (1977) to make comparisons between theory and experiment. From our comparisons we see that the observed groups propagate faster than linear theory predicts.

5. Exact solutions

Equation (4.3) has exact solutions, called solitons, which are progressive envelope pulses of permanent form. It also has similarity solutions for decaying oscillations (radiation) which decay like linear dispersion as $T^{-\frac{1}{2}}$.

In this section we discuss some previously studied solutions to the NLS equation. These known solutions are used to determine the characteristic phase evolution of radiation, soliton and bound state. These characteristic phase evolutions can then be used to classify both observations and numerical solutions.

We examine spatially compact profiles of the form

$$f(X) = \operatorname{sech}(\sqrt{2}\,X/s). \tag{5.1}$$

Using the formula of Yuen & Lake (1975), we find the predicted number of solitons N_s:

$$N_s = \frac{\sqrt{2}}{\pi}\int_{-\infty}^{\infty} f(X)\,\mathrm{d}X = s. \tag{5.2}$$

For integer values of s we get an exact number of solitons. For non-integer s we get solitons plus radiation. When $s < 1$ only radiation is present. The bound state of solitons is predicted when $s \geqslant 2$, since f is real and symmetric (Satsuma & Yajima 1974).

5.1. *Radiation*

We consider an asymptotic state that contains no permanent soliton ($s = \frac{1}{2}$), and whose evolution is dominated by linear dispersion. If we write the complex variable A as

$$A = R\exp(\mathrm{i}\pi p). \tag{5.3}$$

We find that the asymptotic solution behaves like radiation with amplitude and phase modulation given by

$$R(X,T) = A_0\,T^{-\frac{1}{2}}, \tag{5.4a}$$

$$p(X,T) = -\frac{1}{2\pi}\left[\frac{X^2}{T} + A_0^2\ln T + \phi_0\right], \tag{5.4b}$$

where A_0, ϕ_0 are not constants but are slowly varying functions of X/T.

The full solution for initial condition (5.1) with $s = \frac{1}{2}$ is calculated for $-7.5 < X < 7.5$ and $0 < T < 10$. The percentage error calculated from the first conservation law is 0.003 %.

Figures 3(*a*,*b*) show the amplitude and phase modulation at four times. The amplitude decays like $T^{-\frac{1}{2}}$ (with only a small deviation from the asymptotic solution) for $T > 5$, and actually reaches the asymptotic state at $T = 18$. The initial phase modulation is zero. The offset between successive phases (figure 3*b*) is 30 rad. The initial group is centred at $X = 0$ in a frame that propagates at linear group velocity.

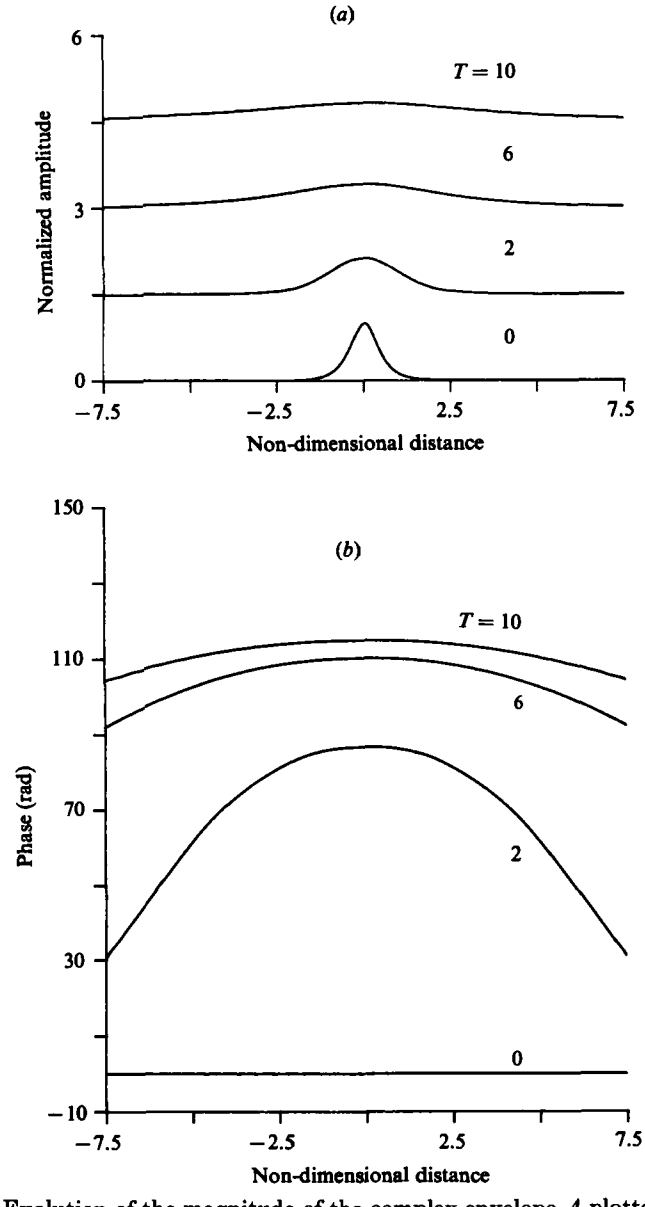

FIGURE 3. (*a*) Evolution of the magnitude of the complex envelope A plotted at 4 successive time steps (time increases upwards) for the $\frac{1}{2}$-soliton solution. Amplitudes are offset by 1.5. (*b*) Evolution of the phase corresponding to (*a*). Phases are offset by 30 rad.

The centre value of the phase decreases with time and exhibits a smooth and symmetric spatial decay from the origin like $-X^2$. This is the principal characteristic of radiation as seen in the phase modulation. It represents the dispersion of wavenumber components in the moving reference frame. In amplitude modulation we see the centreline amplitude decrease whilst the off-centre amplitude increases initially as the group spreads (radiates). The first conservation law indicates that, for radiation, the envelope length increases linearly with time.

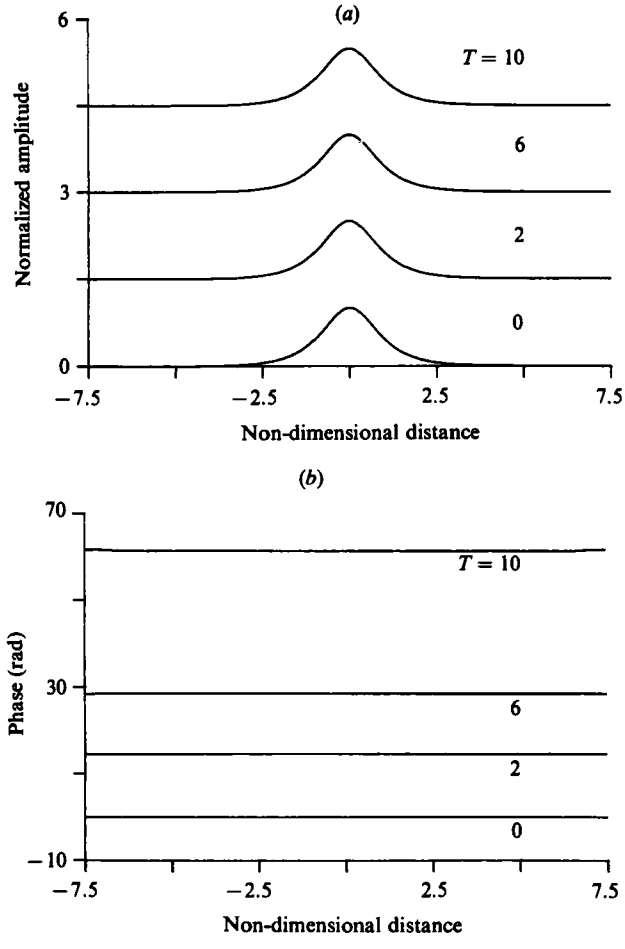

FIGURE 4. (*a*) Evolution of the amplitude for a one-soliton solution. Offset is 1.5. (*b*) Evolution of the phase corresponding to (*a*). Offset is 15 rad.

5.2. *Soliton*

The initial condition (5.1) with $s = 1$ yields an exact one-soliton solution. The evolution is calculated for $-7.5 < X < 7.5$ and $0 < T < 10$. The error is 0.001 %. The asymptotic solution is given by

$$R(X, T) = \operatorname{sech}(\sqrt{2}\, X), \tag{5.5a}$$

$$p(X, T) = -T/4\pi. \tag{5.5b}$$

Figures 4(*a*,*b*) show the amplitude and phase modulation at various time steps. The amplitude modulation shows a steady permanent profile. The phase modulation shows a constant downward shift in time (successive phases are offset by 15 rad).

5.3. *Bound state*

The initial condition is that for the simplest bound state containing two interacting solitons and one recurrence frequency. We specify (5.1) with $s = 2$. The evolution is calculated for $-7.5 < X < 7.5$ and $0 < T < 30$. The first recurrence takes place at $T = 12.6$ (figures 5*a*,*b*).

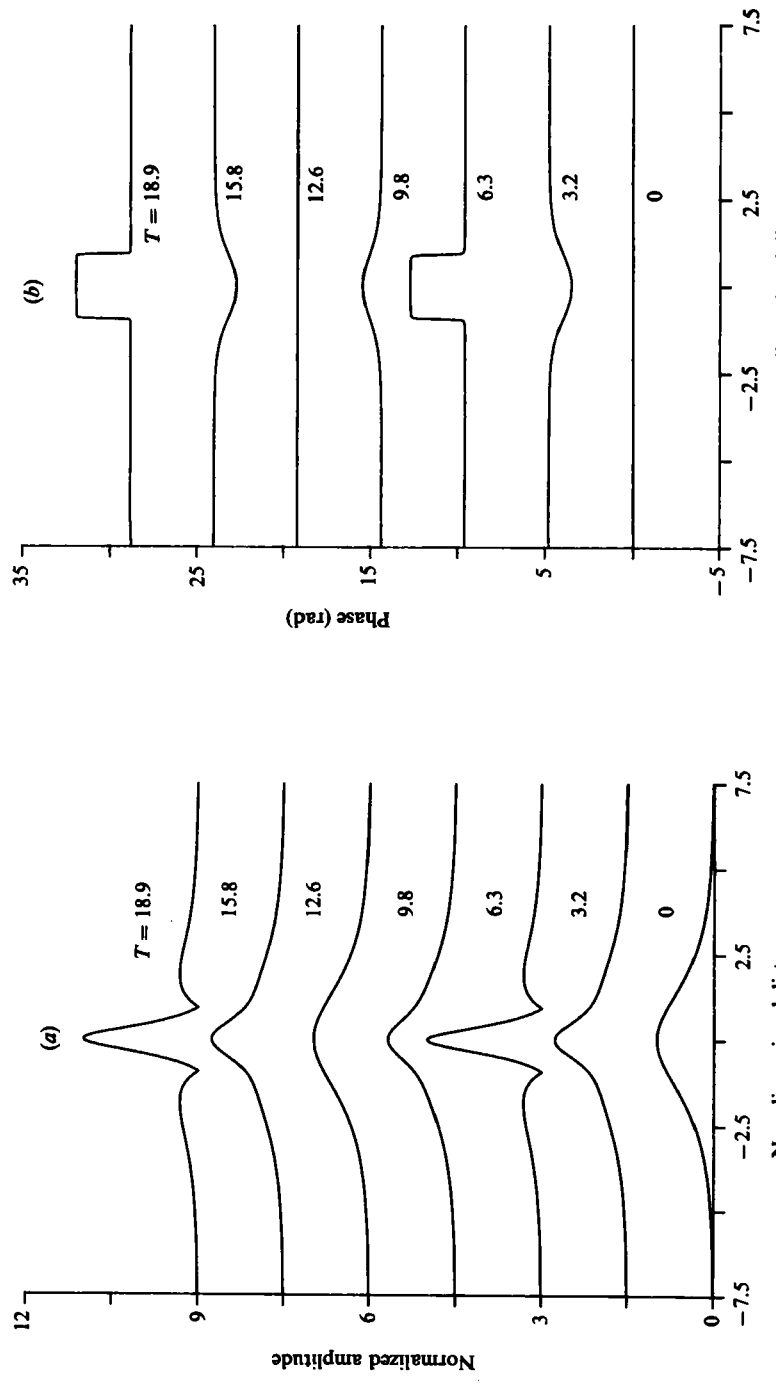

FIGURE 5. (*a*) Amplitude modulation at successive times for a 2-soliton solution. Notice recurrence of initial condition at $T = 12.6$. Offset is 1.5. (*b*) Phase modulation for a 2-soliton solution. Notice jumps at $T = 6.3$ and $T = 18.9$ corresponding to amplitude nodes. Offset is 5 rad.

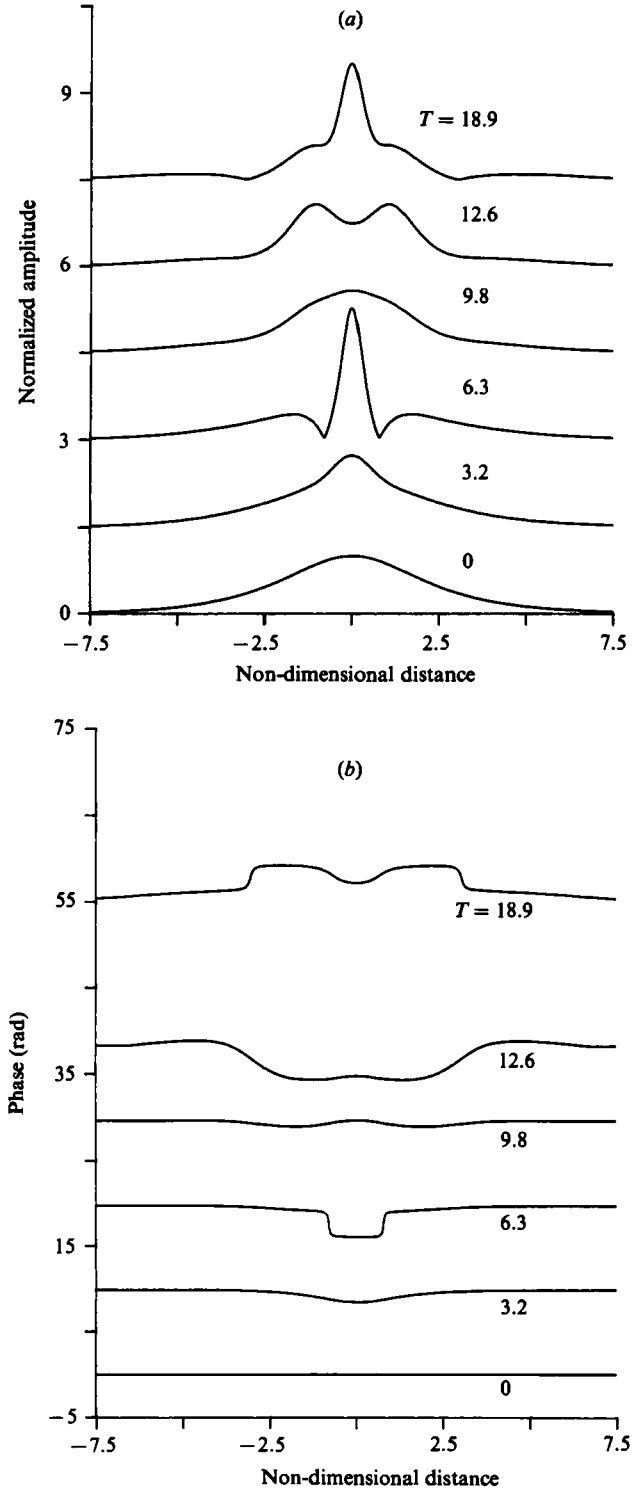

FIGURE 6. (*a*) Evolution of amplitude modulation for a $\frac{5}{2}$-soliton solution. Offset is 1.5. (*b*) Evolution of the phase corresponding to (*a*). Offset is 10 rad.

Figures 5(*a*,*b*) show the amplitude and phase modulations. From the initial condition the soliton evolves to a narrower pulse of twice the height with symmetric sidelobes ($T = 6.3$). Between the sidelobes and the central pulse we see nodes or zeros in amplitude. The initial phase is uniform and zero. The phases are offset by 5 rad. The phase modulates ($T = 3.2$) and then returns to uniform except for two discontinuities: a jump of π connects two sides of nearly constant phase. The jumps occur in X at the location of the amplitude nodes. In the complex plane this means that A has constant phase angle and passes through the origin so that there is no discontinuity in derivative across the node.

The phase modulates again ($T = 9.8$) as the solitons interact to reconstruct the initial condition at $T = 12.6$. The phase is again uniform, but with a small constant phase shift as in the evolution of a one-soliton solution. The oscillation is seen to go back and forth between the two endstates: the initial condition and the narrower, steeper pulse with sidelobes (the minimum and maximum in amplitude modulation, respectively). At each of these two endstates the phase is nearly uniform, with the exception of discontinuities in phase at the nodes of A. The intermediary stages (growing and decaying modulation) between these two endstates also recur ($T = 3.2, 9.8, 15.8$).

5.4. *Bound state plus radiation*

We specify (5.1) with $s = \frac{5}{2}$. The solution is calculated for $-7.5 < X < 7.5$ and $0 < T < 30$. Figures 6(*a*,*b*) show the amplitude and phase modulations at successive times. The evolution is best distinguished by the phase. The phases are offset by 10 rad. We still see the jump of π at the node locations when $T = 6.3$. The background of linear dispersion is evidenced by the spread of the phase at $T = 18.9$. The bound-state interaction is characterized, as in the two-soliton solution, by an oscillation between two endstates of maximum and minimum amplitude modulation. The phase is nearly uniform at the extremes of amplitude modulation ($T = 0, 6.3, 23$) and is modulated during the transitions ($T = 3.2, 18.9, 30$).

5.5. *Divergent solitons*

For our final example we examine the case of divergent solitons for an initial condition of the form

$$f(X) = \operatorname{sech}[\tfrac{1}{2}(\sqrt{2}\,X - 0.6)] - \operatorname{sech}[\tfrac{1}{2}(\sqrt{2}\,X + 0.6)]. \tag{5.6}$$

This case was first examined numerically by Satsuma & Yajima (1974) and is shown in figure 5 of their paper. The initial condition is antisymmetric and yields two divergent solitons of equal amplitude and equal but opposite velocities. Figures 7 (*a*,*b*) show amplitude and phase modulations at successive times. Phases are offset by 20 rad. The phase evolution shows two uniform regions of phase corresponding to the two pulses, with a jump of π connecting the two regions where the amplitude node occurs. The solitons do not interact, as is proved by the amplitude modulation, which is fairly steady, and by the lack of phase modulation. The phase remains uniform in each of the two regions, with slight constant shifts at successive times as in the one-soliton solution.

5.6. *Summary of phase-modulation characteristics*

The soliton evolution is characterized by a locally uniform phase ($p_X = p_{XX} = 0$) with small constant shifts in time. The bound-state evolution is characterized by a locally

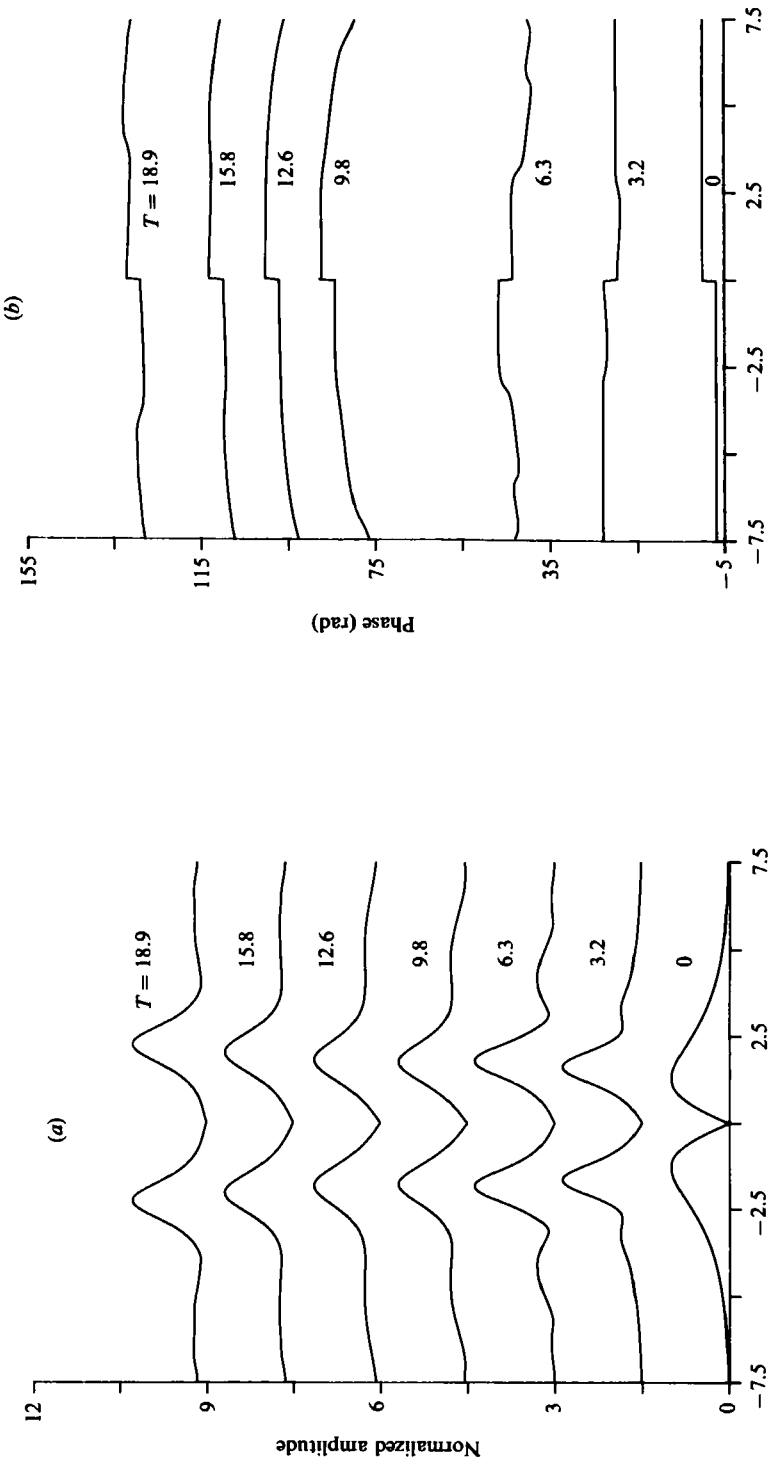

FIGURE 7. (*a*) Evolution of amplitude modulation for divergent solitons. Offset is 1.5.
(*b*) Evolution of the phase corresponding to (*a*). Offset is 20 rad.

uniform phase ($p_X = 0$) at times of minimum and maximum amplitude modulation. Undulations in phase occur during the growth and decay of modulation. Radiation is characterized by a negative curvature in the phase ($p_{XX} < 0$).

6. Comparison with observations

We compare amplitude and phase modulations of the observations at fixed fetches to the numerical solutions at times corresponding to those fetches. The modulations were non-dimensionalized using the scaling given in (4.2), where ω_0, k_0 and maximum A are those measured from the initial condition at 6.1 m. The carrier frequency was removed. The segment of time series at further fetches was chosen by propagating the initial observation down the channel at the linear group velocity. The NLS evolution is in a frame moving at linear group velocity. From such a comparison we observe that the groups travel faster than linear theory predicts.

The numerical solutions have more points than the Hilbert-transform length. Hence the beginning and end of the observations are padded by the same constant value that matches to the start of the group, with ends tapered to zero. The time interval for evolution is chosen to correspond to the length of evolution in the wave channel (scaled by group velocity and steepness).

The comparisons at each fetch are not exact. First, there is an error introduced in using the linear group velocity. Secondly, the time chosen is taken to be the closest grid point to the exact time calculated using linear group velocity. What we hope to illustrate here is the overall character of the phase evolution based on insight gained from the exact solutions. From amplitude modulation we can estimate the timescale on which dissipation becomes important. The effect of dissipation can also be seen in the change in character of the phase evolution between damped and undamped numerical results.

To model the effects of dissipation, (4.3) was modified to the form

$$\mathrm{i}A_T - \tfrac{1}{8}A_{XX} - \tfrac{1}{2}|A|^2 A = -\mathrm{i}\alpha A. \tag{6.1}$$

The coefficient α was estimated from observations as in Chu & Mei (1971). The values of α are listed in table 1. The method for estimating α is found in Appendix B.

6.1. *Radiation*

We calculate the evolution of a group of ten waves of small wave steepness ($ak = 0.03$, $f_0 = 0.80$ Hz, $f_1 = 0.80$ Hz) for $|X| < 9.0$ and $0 < T < 2.5$. The group evolution is dominated by linear dispersion. The lengthening of the group is linear in T.

A comparison of the amplitude modulations (figures 8*a–c*) shows that the observed group is strongly attenuated. The comparison between observations (figure 8*a*) and the undamped model (figure 8*b*) is quite good at 15.2 m and 30.5 m (not shown). (Note that the numerical solutions are labelled by fetch; actually they are the times of the solution that correspond to those fetches.) The effect of the damping becomes somewhat evident at 45.7 m, and more markedly in the subsequent evolution. The inclusion of a constant modulus of decay (figure 8*c*), estimated from the observations, gives good agreement for the entire evolution (137.2 m). There is no suggestion of soliton behaviour in the amplitude modulation, nor is any predicted for this initial group using (5.2).

The initial phase is basically constant ($p_X = p_{XX} = 0$) within the group. The

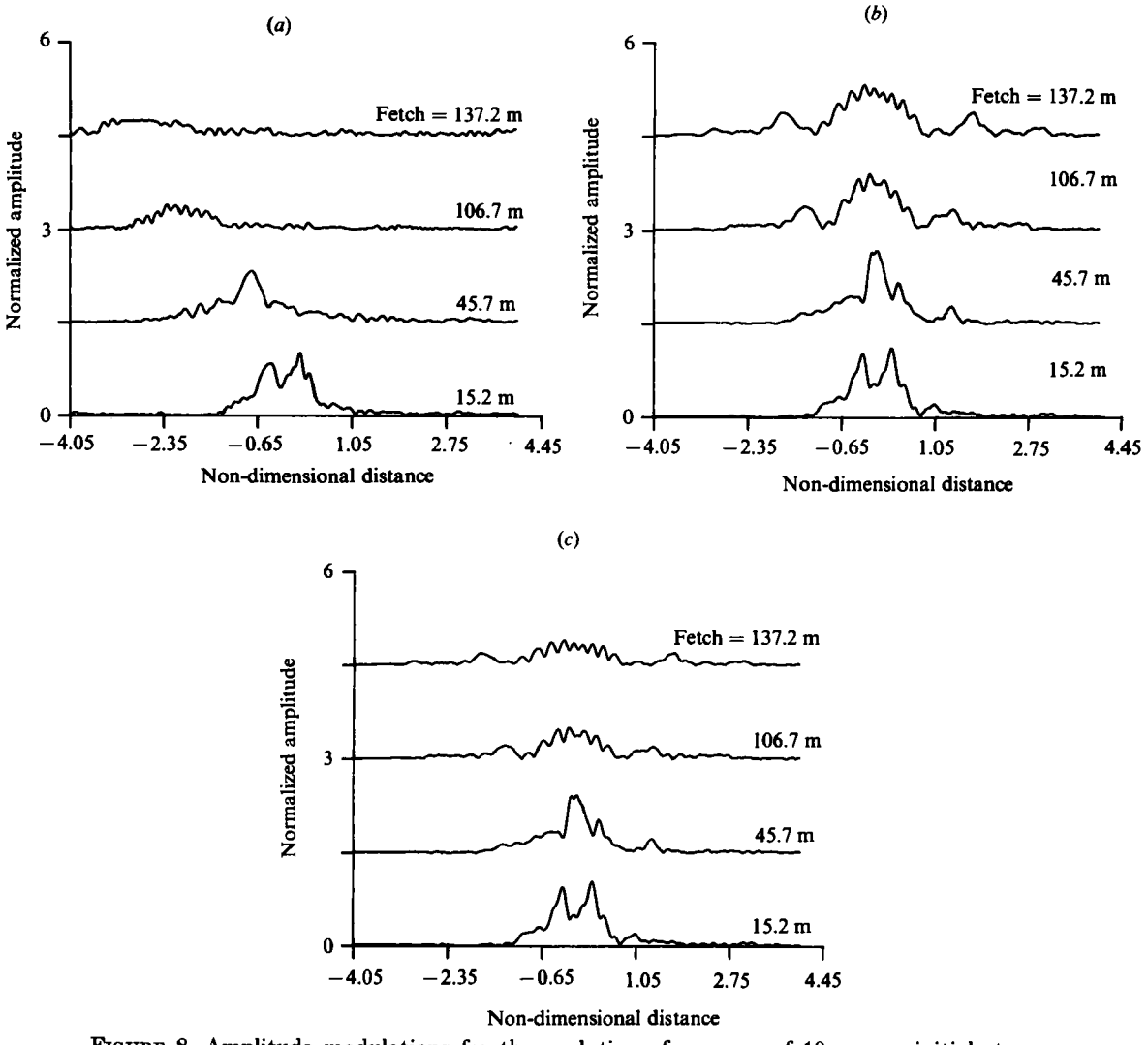

FIGURE 8. Amplitude modulations for the evolution of a group of 10 waves, initial steepness $ak = 0.03$. Offset is 1.5. (*a*) Observations, non-dimensionalized at each fetch by the initial-condition scaling. (*b*) Undamped NLS solutions at times corresponding to the fetches in (*a*). (*c*) Damped NLS solution at times corresponding to the fetches in (*a*).

phase modulations for the observations (figure 9*a*) and for both numerical solutions (figures 9*b*,*c*) agree, both in general character and, at early fetches (time steps), in detail. The phases are shown stacked with an offset of 35 rad.

The phase evolves from initial uniformity (6.1 m) imposed by the wavemaker to a state characteristic of radiation ($p_{XX} < 0$). The evolution thus seems to consist of an initial forced pulse that disperses linearly. The amplitude and phase of observations clearly show that the group has components moving at a rate faster than the linear group velocity based on the initial carrier frequency.

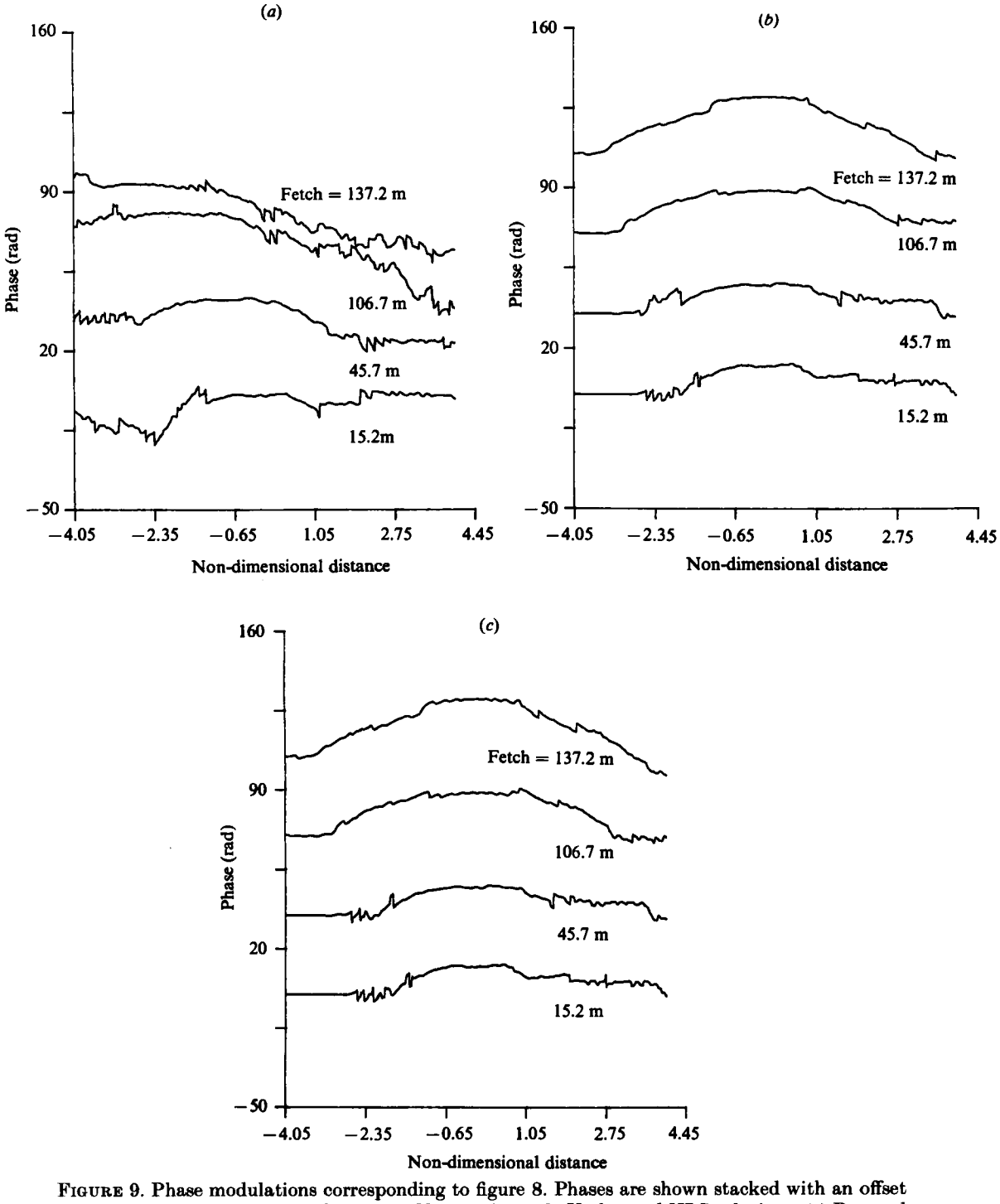

FIGURE 9. Phase modulations corresponding to figure 8. Phases are shown stacked with an offset of 35 rad between successive phases. (*a*) Observations. (*b*) Undamped NLS solutions. (*c*) Damped NLS solutions.

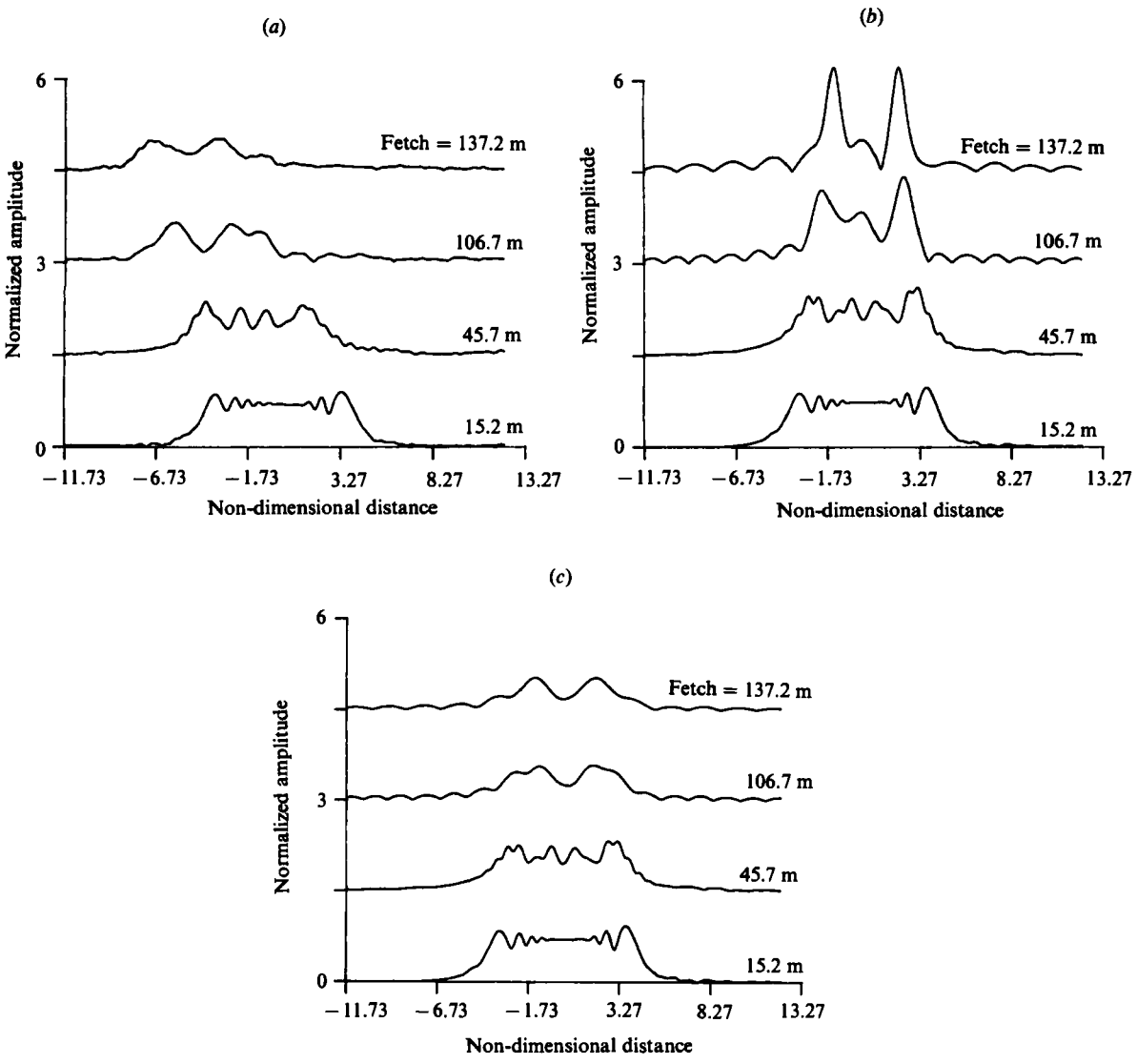

FIGURE 10. Amplitude modulations for the evolution of a group of 25 waves, initial steepness $ak = 0.10$. Offset is 1.5. (*a*) Observations, nondimensionalized at each fetch by the initial-condition scaling. (*b*) Undamped NLS solutions at times corresponding to the fetches in (*a*). (*c*) Damped NLS solution at times corresponding to the fetches in (*a*).

6.2. *Bound state plus radiation*

An example of soliton-like behaviour is shown in figures 10 and 11 for a longer group of 25 waves with initial steepness $ak = 0.10$, $f_0 = 0.96$ Hz and $f_1 = 0.94$ Hz. The predicted number of solitons is 2.3.

The amplitude modulations are plotted in figures 10(*a–c*). The observations (figure 10*a*) and the damped solution (figure 10*c*) agree very well. Damping becomes important at 76.2 m, seen by comparison with the undamped solution.

The phase modulations are shown in figures 11 (*a–c*). The offset between successive phases is 35 rad. The observations (figure 11*a*) show the phase evolution characteristic

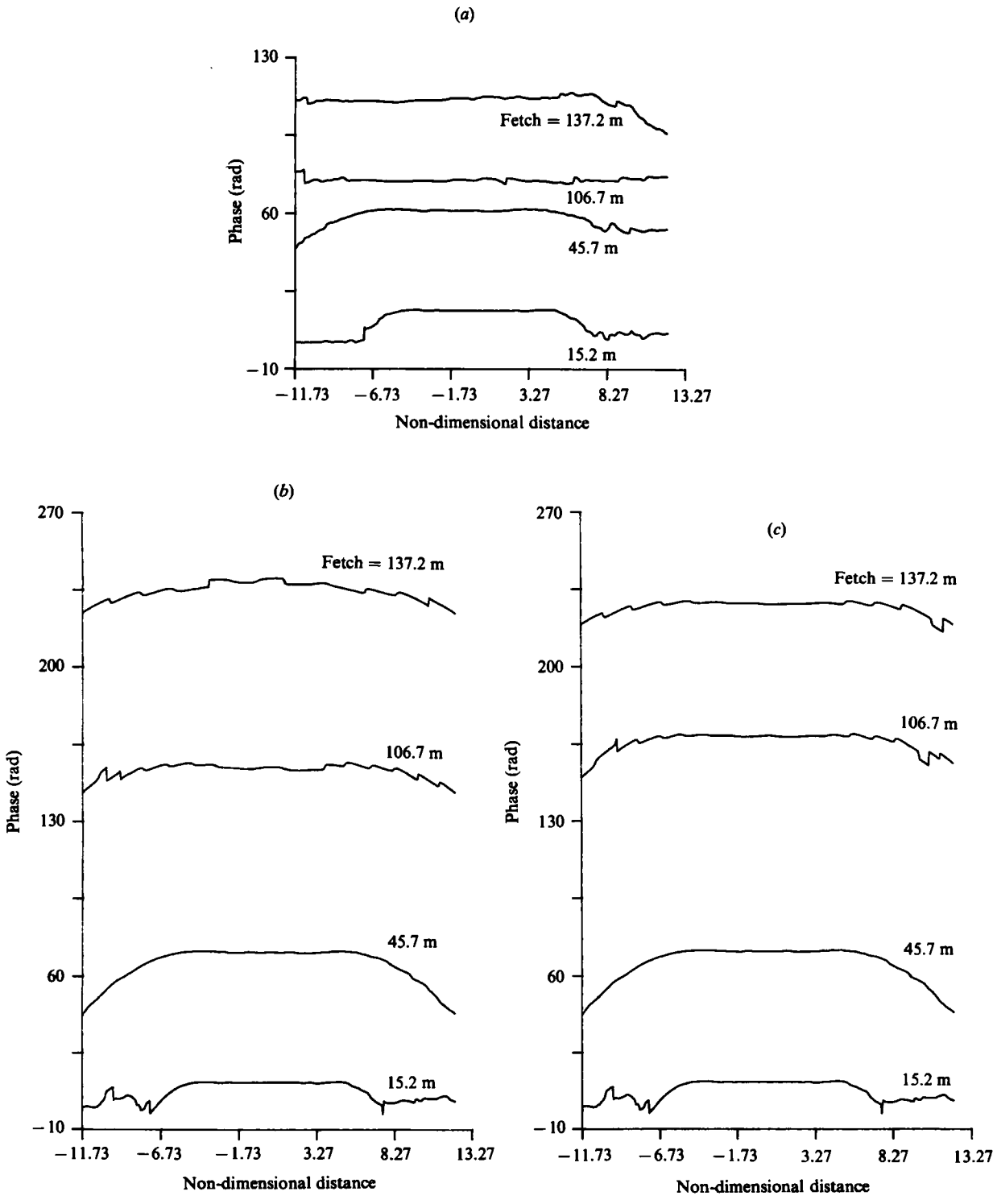

FIGURE 11. Phase modulations corresponding to figure 10. Phases are shown stacked with an offset of 35 rad between successive phases. (*a*) Observations. (*b*) Undamped NLS solutions. (*c*) Damped NLS solutions.

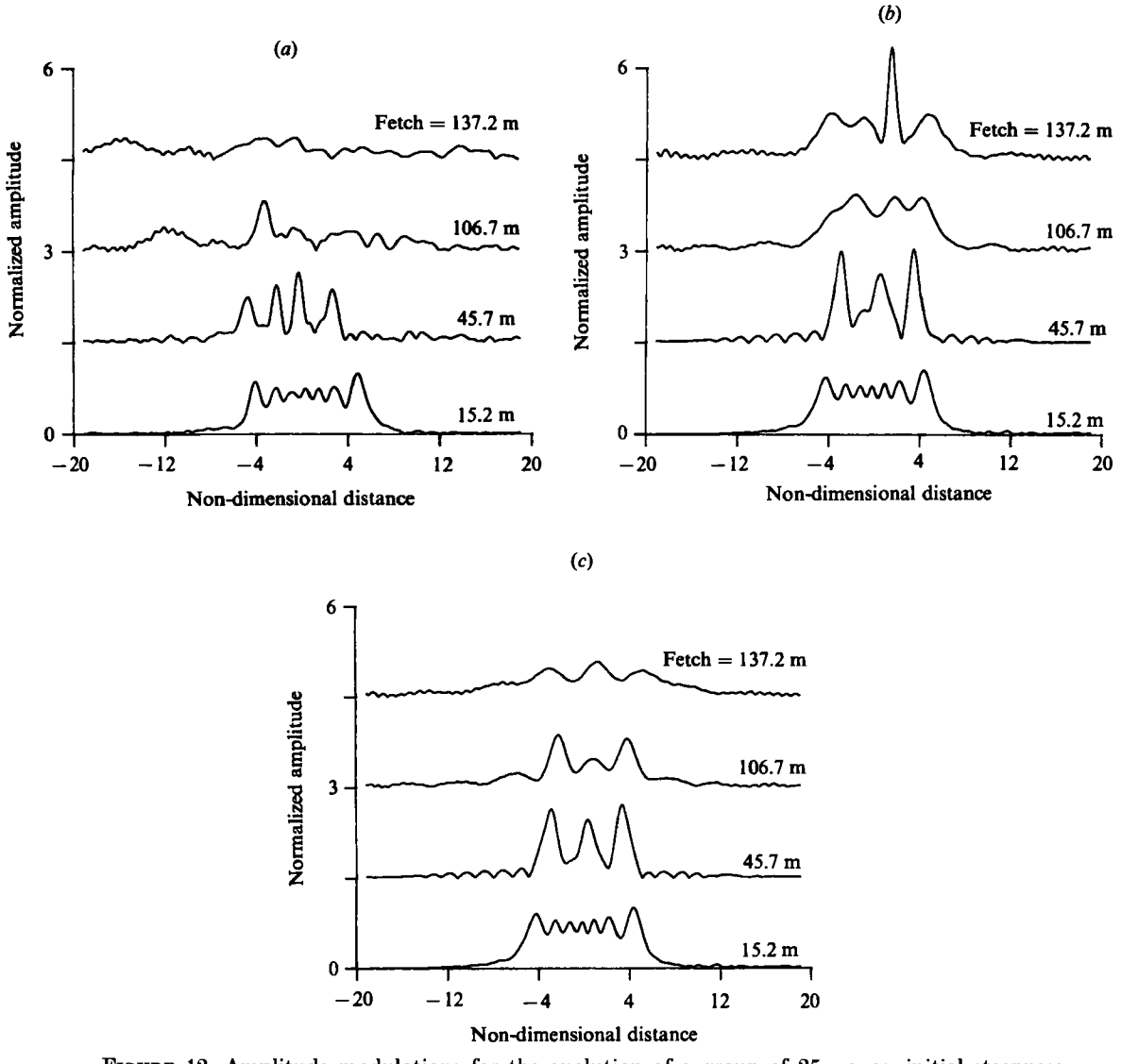

FIGURE 12. Amplitude modulations for the evolution of a group of 25 waves, initial steepness $ak = 0.16$. Offset is 1.5. (*a*) Observations, nondimensionalized at each fetch by the initial-condition scaling. (*b*) Undamped NLS solutions at times corresponding to the fetches in (*a*). (*c*) Damped NLS solution at times corresponding to the fetches in (*a*).

of a soliton. The phase is basically uniform ($p_X = p_{XX} = 0$) with small shifts at successive fetches. There are small undulations in the phase. The initial jump in phase occurs at the ends of the group where there are amplitude nodes. At the edges of the group we see radiation ($p_{XX} < 0$). The undamped phase evolution (figure 11*b*), as in the last example, is initially uniform ($p_X = p_{XX} = 0$) like a soliton or bound state. Beginning at 76.2 m, where dissipation is first noticeable, rather than remain uniform as do the observations and the damped numerical solution, the undamped solution modulates (figure 11*b*). Particularly at 137.2 m, the phase modulation resembles the $\frac{5}{2}$-soliton solution at $T = 18.9$ (figure 6*b*). The phase is like that of the bound soliton

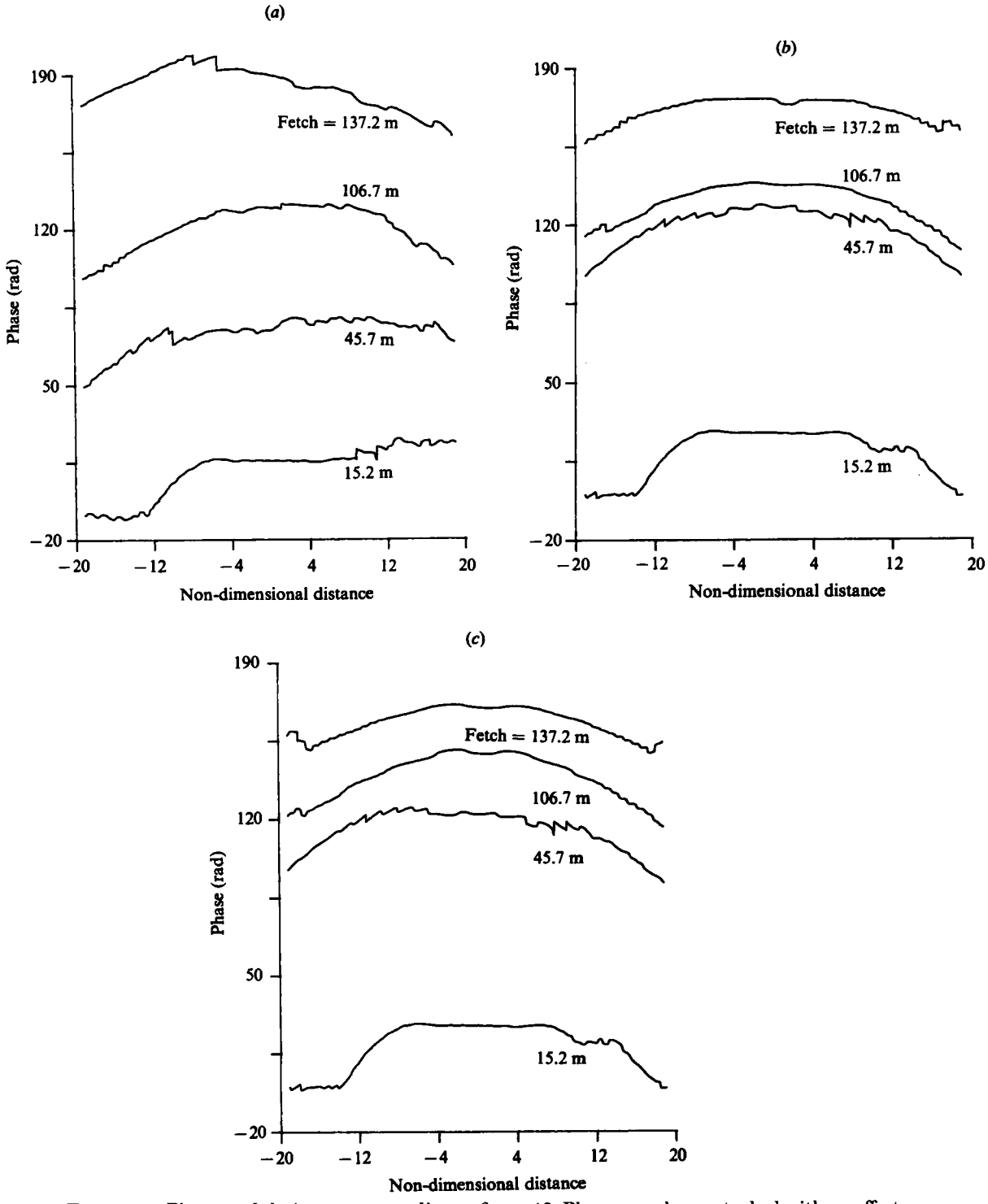

FIGURE 13. Phase modulations corresponding to figure 12. Phases are shown stacked with an offset of 52.5 rad between successive phases. (*a*) Observations. (*b*) Undamped NLS solutions. (*c*) Damped NLS solutions.

as it approaches a maximum modulation. The jumps in phase occur within the group at amplitude minima or nodes.

The last example we discuss is that of the longest (25 waves) steepest wave group ($ak = 0.16$, $f_0 = 1.21$ Hz and $f_1 = 1.01$ Hz). Figures 12 and 13 compare the modulations. The predicted number of solitons was 5.2; the observed number was 4.

Amplitude modulations (figures 12*a–c*) show reasonable agreement between observations and the damped NLS solution. The phase modulations are shown in figures 13(*a–c*). The offset between successive phases is 52.5 rad. Notice in figure 13(*a*) the marked negative curvature at 15.2 m at the front of the group, corresponding to leading low-frequency dispersion. Within the group at 15.2 m the phase has remained very flat. At 45.7 m we see the small local phase reversals occurring near amplitude minima. The small undulations in phase are characteristic of growing and decaying modulation. The phase is much more uniform again at 137.2 m. (Between -12 and -4 non-dimensional distance we see a jump of 2π and 4π missed by the unwrapping technique – continuous phases shown here are all 'unwrapped' from principal values of the arctangent function). There is a background of radiation. The numerical solutions (figures 13*b–c*) also exhibit the bound-state characteristics.

Although the bound-state phase modulation cannot be distinguished from bound state plus radiation, it is different from pure radiation and simple soliton behaviour. What we observe is characteristic of an ongoing interaction of some kind, which in amplitude is shown by growing and decaying modulation. The phase is further evidence that it is indeed an interaction and not linear dispersion by its relative flatness ($p_{XX} = 0$) within the group with small reversals located at amplitude minima. The phase also seems distinguishable from that of divergent solitons in that the reversals change in time, generally corresponding to locations of nodes, rather than staying fixed in relative position in the group.

7. Conclusions

We have made comparisons between observations and numerical solutions of narrow-banded wave-group evolution. From these comparisons, using the long-time behaviour of exact asymptotic solutions as a guide, we believe that we can distinguish between radiation (linear dispersion) and soliton-like behaviour based on characteristics of the phase modulation. This does not appear to have been analysed before in observations. We suggest that, at least for wave groups with a well-defined carrier frequency, the phase modulation may give a clearer indication of the type of wave interaction that takes place.

Owing to dissipation, it seems that recurrence does not take place. However, in contrast with predictions of the linear theory for the thermalization of the group, the wave groups do remain coherent throughout their development. The phase modulation indicates that the waves remain together and interact in the long-time evolution.

We find that the damped NLS equation models the long-time evolution surprisingly well in view of the weak nonlinearity of the theory and the crudeness of the dissipation term. Although the form of the dissipation does not directly affect the phase, we find there is an indirect effect on the phase in the long-time evolution by a change in the 'quantum' or number of observed groups.

Although the NLS model seems to describe the global character of the amplitude and phase modulation, we observe jumps in the frequency modulation and reversals in phase which are not described by weakly nonlinear theory. It is suggested that these jumps are related to the mechanism of frequency downshifting. It is also

observed that the groups propagate faster than linear theory predicts, probably because of both nonlinear effects and the downshift in frequency. In a statistical sense the jumps are rare, yet they are dynamically significant since their effect is irreversible and cumulative.

The experiments were made in the outdoor flood plain at Bay St Louis, Mississippi, with the cooperation of Dr M.-Y. Su of NORDA. P. Marler and R. Myrick helped with the experiments. We thank K. Melville and C. C. Mei for useful suggestions, and G. Sahar for generously providing his software. Comments from reviewers made substantial improvements on the original manuscript. T.K.C. acknowledges the support of a grant from the U.K. Natural Environment Research Council while this paper was written. The research was sponsored by ONR under contract N00014-80-C-0273.

Appendix A. Hilbert transform

We follow the discussion in Melville (1983). For further detail the interested reader is referred to his paper and to Sahar (1981).

If $g(t)$ is a real function of time, $-\infty < t < \infty$, then we define the analytic function

$$h(t) = g(t) - \mathrm{i}\hat{g}(t), \tag{A 1}$$

where

$$\hat{g}(t) = \mathrm{HT}[g(t)] \equiv \frac{1}{\pi}\int_{-\infty}^{\infty} \frac{g(t')\,\mathrm{d}t'}{t-t'} \tag{A 2}$$

(HT [ ] denotes the Hilbert transform of [ ]).

If we represent our real measured time series $g(t)$ as a Fourier series

$$g(t) = \mathrm{Re}\left\{\sum_{n=0}^{\infty} a_n \exp[\mathrm{i}\phi_n]\right\}, \tag{A 3}$$

where a_n and ϕ_n are respectively the amplitude and phase of the nth Fourier component, then by the properties of the Hilbert transform

$$\mathrm{HT}[g(t)] = -\mathrm{Im}\left\{\sum_{n=0}^{\infty} a_n \exp[\mathrm{i}\phi_n]\right\}. \tag{A 4}$$

In general, if our data are given as

$$g(t) = \mathrm{Re}\{a(t)\exp[\mathrm{i}\phi(t)]\} \tag{A 5}$$

then we define the analytic function $h(t)$:

$$h(t) \equiv g(t) - \mathrm{i}\hat{g}(t) = a(t)\exp[\mathrm{i}\phi(t)]. \tag{A 6}$$

The amplitude $a(t)$ is given by

$$a(t) = [g^2 + \hat{g}^2]^{\frac{1}{2}}, \tag{A 7}$$

and the phase $\phi(t)$ is given by

$$\phi(t) = \arctan[-\hat{g}/g]. \tag{A 8}$$

If we think of our analytic function as the product of a rapidly varying carrier wave and a slowly varying modulation,

$$h(t) = a(t)\exp[\mathrm{i}\phi(t)] = a(t)\exp\{\mathrm{i}[\theta(t) + \omega_0 t]\}, \tag{A 9}$$

then the complex envelope is described by

$$A(t) = a(t) \exp[\mathrm{i}\theta(t)], \tag{A 10}$$

where a is defined as the amplitude modulation and θ is defined as the phase modulation.

The phase modulation θ is given by

$$\theta = \phi - \omega_0 t = \arctan\left[-\frac{\hat{g}}{g}\right] - \omega_0 t. \tag{A 11}$$

However, the phase modulation is a continuous function of time, whereas the arctangent is restricted to the interval $[-\frac{1}{2}\pi, \frac{1}{2}\pi]$. Instead of using the arctangent, we actually solve for the cosine and sine of ϕ, which extends our interval to $[-\pi, \pi]$. The phase is unwrapped by looking for and removing discontinuities of 2π.

Use of this transform method implies a weakly narrow-banded assumption. The bandwidth of the spectrum is required to be less than or equal to $2\omega_0$.

Appendix B. Dissipation

The wave-amplitude decay coefficient α is determined following the approach outlined in Chu & Mei (1971). First we define a wave-packet energy

$$E_{\mathrm{p}}(x) = \int_{-\infty}^{\infty} a^2(x,t)\, \mathrm{d}t, \tag{B 1}$$

where $a(x,t)$ is the wave amplitude expressed as a function of location x and time t. A damping coefficient σ for the packet energy is estimated from the energy equation

$$\left\{\frac{\partial}{\partial t} + C_{\mathrm{g0}} \frac{\partial}{\partial x}\right\} a^2 = -\sigma a^2, \tag{B 2}$$

where C_{g0} is the linear group velocity. Integrating first with respect to t and then with respect to x (from our initial observation at x_0) yields

$$\sigma = \frac{-C_{\mathrm{g0}}}{x - x_0} \ln \frac{E_{\mathrm{p}}(x)}{E_0}, \tag{B 3}$$

where E_0 is the packet energy at x_0. In obtaining (B 3) we have used the property that $a(x, \pm\infty) = 0$ at a fixed location x for a finite wave group. We find that the packet energy decays as σ/C_{g0}. We determine the amplitude decay coefficient to be

$$\alpha = \sigma / 2C_{\mathrm{g0}}. \tag{B 4}$$

The estimate of α is made from a linear regression of $\ln(E_{\mathrm{p}}/E_0)$ versus $x - x_0$. The values for each experiment are listed in table 1.

For the numerical evolutions the decay coefficient was converted from the space domain to the time domain using linear group velocity, i.e. $\frac{1}{2}\sigma$ was used. The dissipation was non-dimensionalized according to (4.2) by $\epsilon^2\omega_0$.

REFERENCES

BENJAMIN, T. B. & FEIR, J. E. 1967 The disintegration of wave trains on deep water. Part 1. Theory. *J. Fluid Mech.* **27**, 417–430.

CHU, V. H. & MEI, C. C. 1970 On slowly-varying Stokes waves. *J. Fluid Mech.* **41**, 873–887.

CHU, V. H. & MEI, C. C. 1971 The nonlinear evolution of Stokes waves in deep water. *J. Fluid Mech.* **47**, 337–351.

FEIR, J. E. 1967 Discussion: some results from wave pulse experiments. *Proc. R. Soc. Lond.* A **299**, 54–58.

KAY, S. M. & MARPLE, S. L. 1981 Spectrum analysis: a modern perspective. *Proc. IEEE* **69**, 1380–1419.

LAKE, B. M. & YUEN, H. C. 1978 A new model for nonlinear wind waves. Part 1. Physical model and experimental evidence. *J. Fluid Mech.* **88**, 33–62.

LAKE, B. M., YUEN, H. G., RUNDGALDIER, H. & FERGUSON, W. E. 1977 Nonlinear deep water waves: theory and experiment. Part 2. Evolution of a continuous wavetrain. *J. Fluid Mech.* **83**, 49–74.

MELVILLE, W. K. 1982 The instability and breaking of deep water waves. *J. Fluid Mech.* **115**, 165–185.

MELVILLE, W. K. 1983 Wave modulation and breakdown. *J. Fluid Mech.* **128**, 489–506.

MOLLO-CHRISTENSEN, E. & RAMAMONJIARISOA, A. R. 1982 Subharmonic transitions and group formation in a wind wave field. *J. Geophys. Res.* **87**, 5699–5717.

PEREGRINE, D. H. 1983 Water waves, nonlinear Schrödinger equations and their solutions. *J. Austral. Math. Soc.* B **25**, 16–43.

RAMAMONJIARISOA, A. R. & MOLLO-CHRISTENSEN, E. 1979 Modulation characteristics of sea surface waves. *J. Geophys. Res.* **84**, 7769–7775.

SAHAR, G. 1981 Modulation of sea surface waves: observations and processing methods. M.S. thesis, Massachusetts Institute of Technology.

SATSUMA, J. & YAJIMA, N. 1974 Initial value problems of one-dimensional self-modulation of nonlinear waves in dispersive media. *Prog. Theor. Phys. Suppl.* **55**, 284–306.

SU, M.-Y. 1982 Evolution of groups of gravity waves with moderate to high steepness. *Phys. Fluids* **25**, 2167–2174.

YUE, D. K.-P. 1980 Numerical study of Stokes' wave diffraction at grazing incidence. Ph.D. thesis, Massachusetts Institute of Technology.

YUEN, H. C. & LAKE, B. M. 1975 Nonlinear deep water waves: theory and experiment. *Phys. Fluids* **18**, 956–960.

ZAKHAROV, V. E. 1968 Stability of periodic waves of finite amplitude on the surface of a deep fluid. *J. Appl. Mech. Tech. Phys.* **9**, 190–194.

ZAKHAROV, V. E. & SHABAT, A. B. 1972 Exact theory of two-dimensional self-focusing and one-dimensional self-modulation of waves in nonlinear media. *Sov. Phys. JETP* **34**, 62–69.